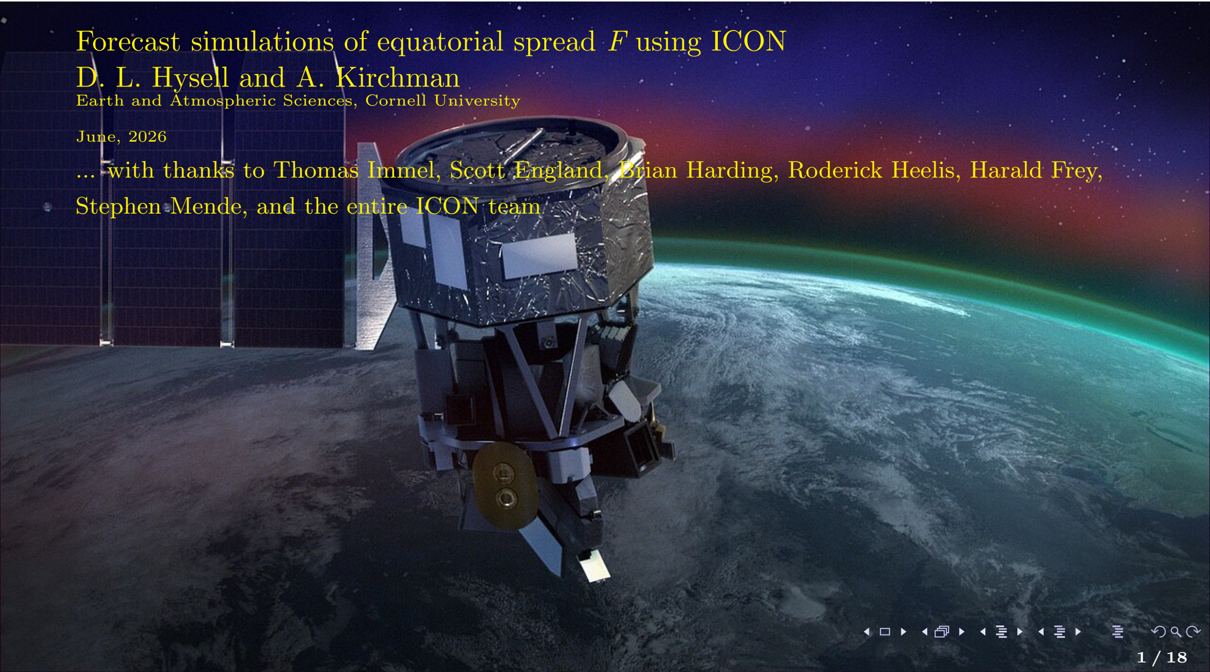

Forecast simulations of equatorial spread F using ICON

D. L. Hysell and A. Kirchman
Earth and Atmospheric Sciences, Cornell University

June, 2026

... with thanks to Thomas Immel, Scott England, Brian Harding, Roderick Heelis, Harald Frey, Stephen Mende, and the entire ICON team

~90 years of equatorial ionospheric space weather

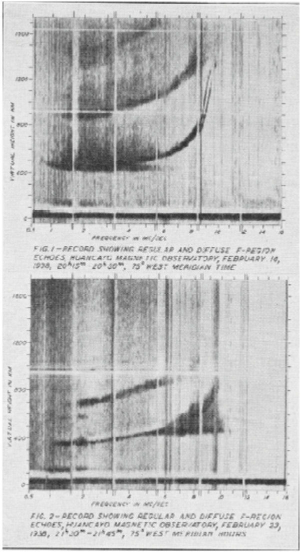

Booker and Wells, 1938

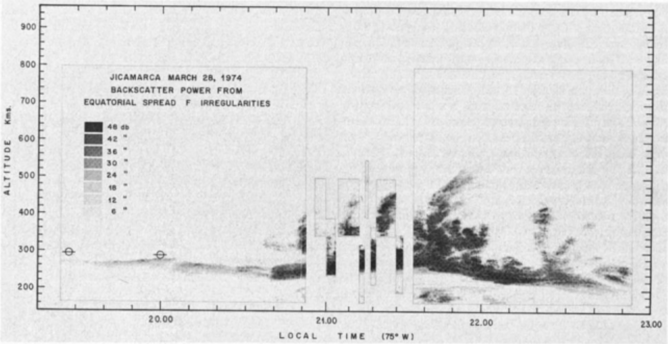

Farley et al., 1970
Haerendel, 1973
Woodman and La Hoz, 1976

ALTAIR radar imagery

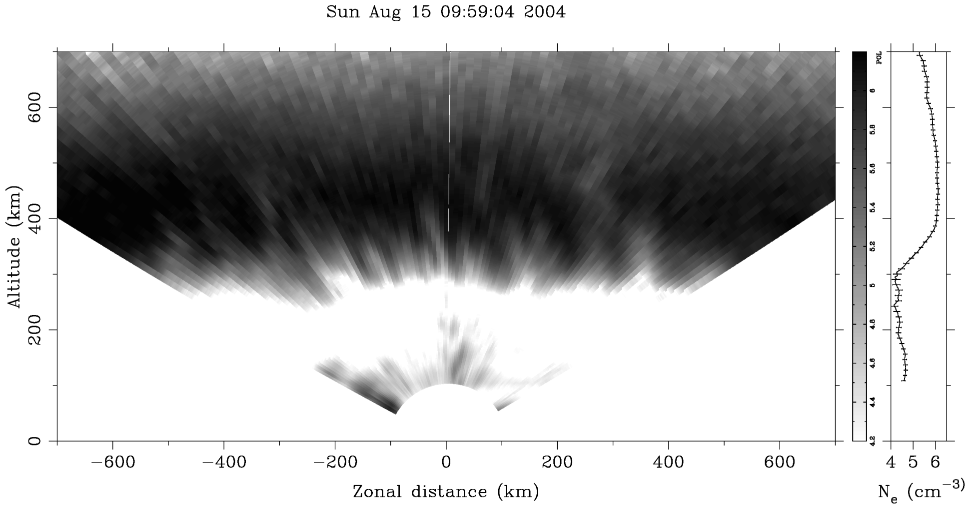

Jicamarca radar imagery

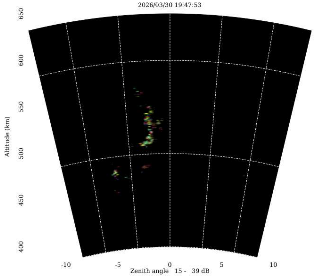

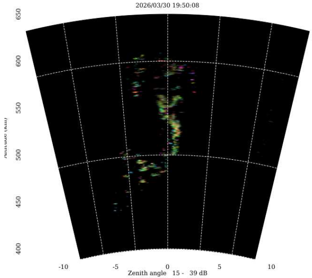

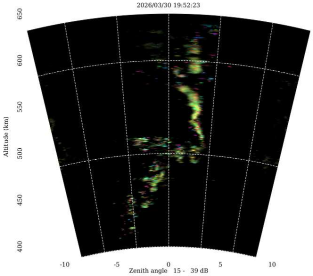

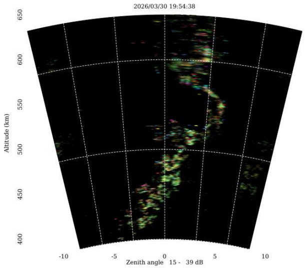

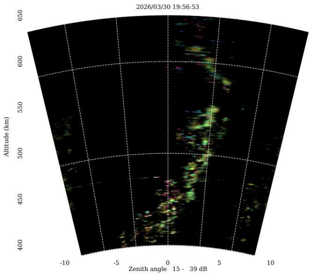

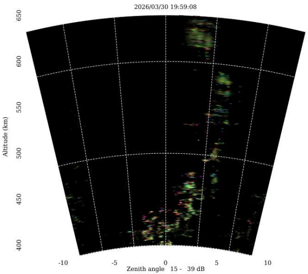

linear analysis (cold fluid plasma) Guzdar et al. [1982]

Assume solutions of the form $\exp(i\omega t - ikx)$

$$\frac{d^2}{dz^2}\phi + p\frac{d}{dz}\phi + q\phi \quad \equiv \quad \mathcal{L}\phi \;=\; 0$$

where z is the vertical direction and

$$\begin{aligned} p(z) \quad &\equiv \quad \frac{n_\circ'}{n_\circ}\left(1 - \frac{i\nu_{\text{in}}}{\tilde{\omega} + i\nu_{\text{in}}}\frac{kV_\circ}{\tilde{\omega}}\right) \\ q(z) \quad &\equiv \quad -k^2 + \frac{kV_\circ}{\tilde{\omega} + i\nu_{\text{in}}}\left(\frac{V_\circ''}{V_\circ} + \frac{gk}{\tilde{\omega}V_\circ}\frac{n_\circ'}{n_\circ} + \frac{V_\circ'}{V_\circ}\frac{n_\circ'}{n_\circ} - \frac{i\nu_{\text{in}}}{\tilde{\omega}}\left\{\frac{n_\circ''}{n_\circ} + \frac{\omega}{\tilde{\omega}}\frac{n_\circ'}{n_\circ}\frac{V_\circ'}{V_\circ}\right\}\right) \end{aligned}$$

allwing for $n(z)$ and $V_\circ(z)$ and with $\tilde{\omega} \equiv \omega - kV_\circ(z)$.

Is $\boxed{\mathcal{L}\mathcal{L}^*\phi = \mathcal{L}^*\mathcal{L}\phi}$?

see e.g. Trefethen et al. 1993.

warm, anisotropic plasmas; plan view

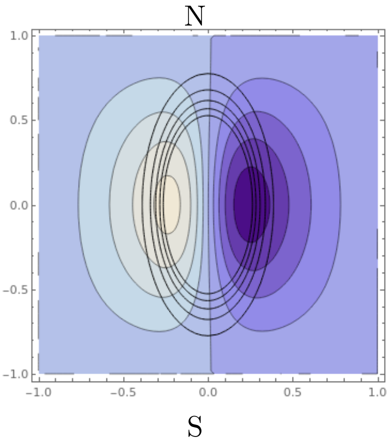

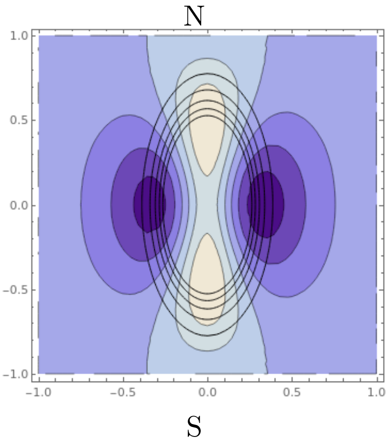

Drake and Huba [1987]

numerical simulations at 35 min., 110 min.

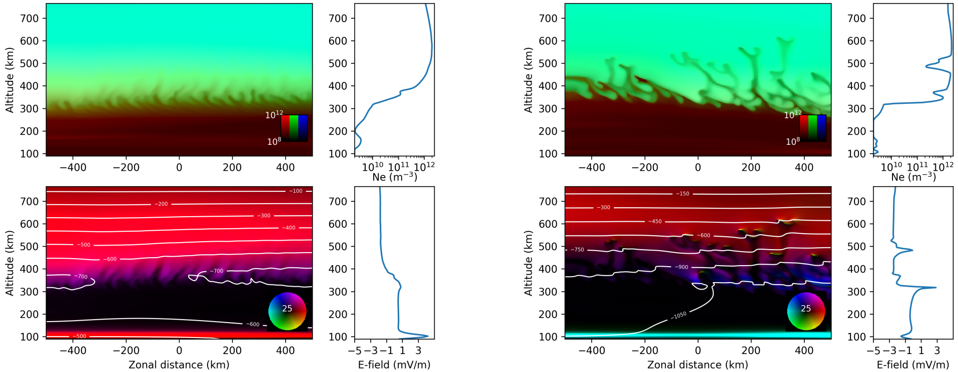

data selection

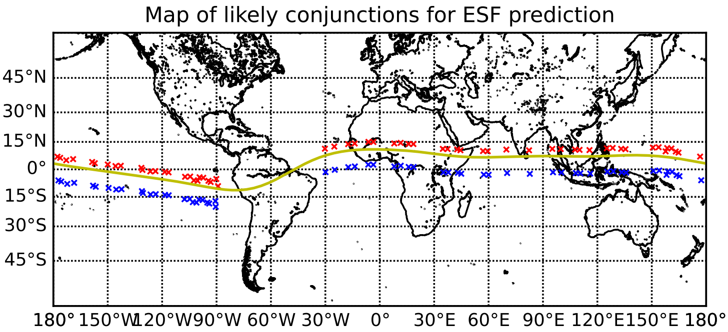

Selected orbital segments for Aug. and Oct., 2022. Blue and red crosses represent forecast (a) and validation (b) segments, respectively.

representative data

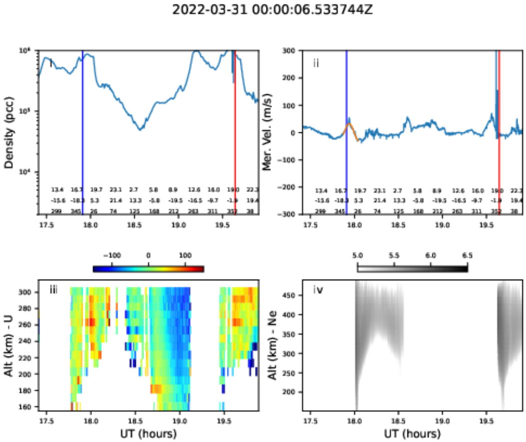

ICON data for Mar. 31, 2022, spanning the first selected orbital segments (a) and (b). (i) IVM-A electron density. (ii) IVM-A perpendicular meridional drift. (iii) MIGHTI red-line zonal winds ($V \in \pm 150$ m/s). (iv) FUV electron density profiles (cgs log $N_e \in 5 - 6.5$). Segments (a) and (b) are indicated by blue and red vertical lines through the IVM-A data, respectively. Text in the rows of text in the top panels indicate solar local time, magnetic latitude, and longitude, respectively, from top to bottom.

ESF events

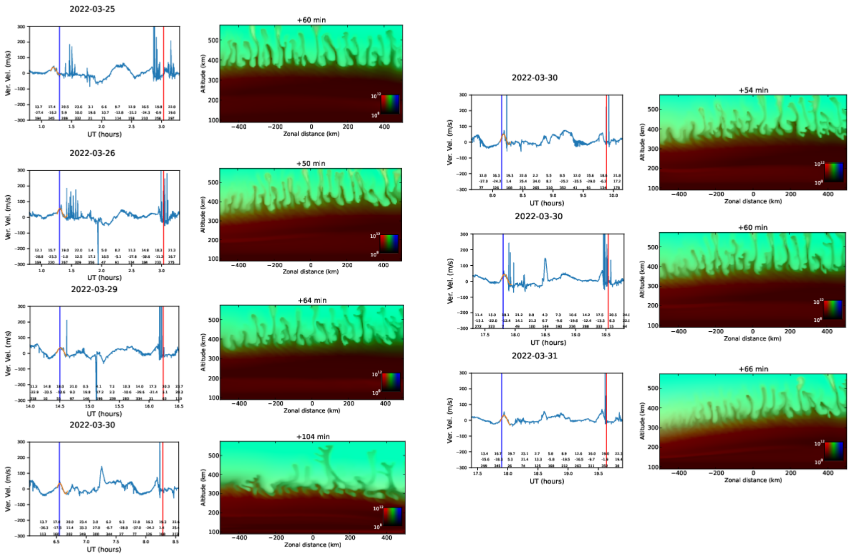
2022-03-25
+60 min
2022-03-26
+50 min
2022-03-29
+64 min
2022-03-30
+104 min
2022-03-30
+54 min
2022-03-30
+60 min
2022-03-31
+66 min
Ver. Vel. (m/s)
UT (hours)
Altitude (km)
Zonal distance (km)

non-ESF events

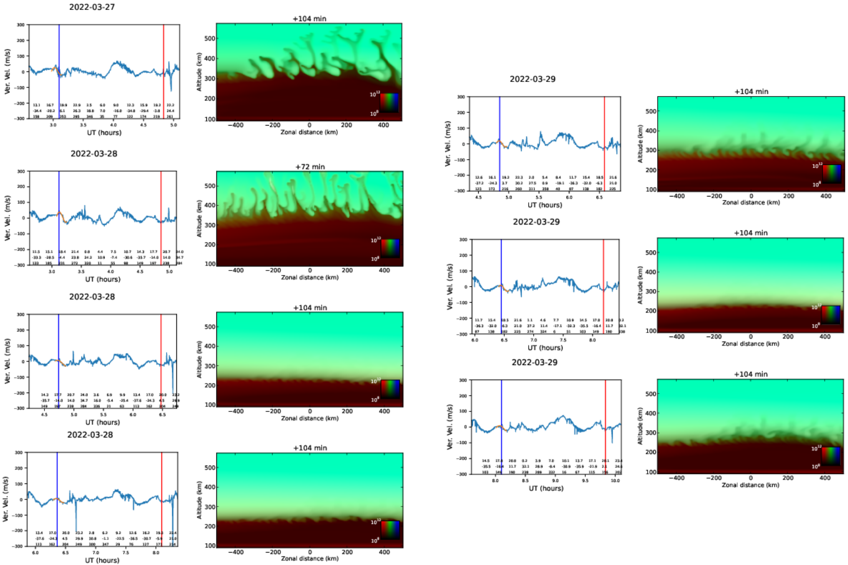

simulation results

Date UT	Time UT	Long. deg.	$V_\circ$ m/s	τ hr.	$t_\circ$ hr.	c m/s	α hr^{-1}	β	N_m cm^{-3}	h_m km	h_1 km	h_2 km	ESF obs.	ESF pred.
3/25	1.22	260	23.8	2.91	18.0	14.3	0.39	-0.15	9.7E5	382	225	46	Y	Y
3/26	1.30	253	29.0	2.38	18.1	27.7	0.26	0.29	2.0E6	337	52.4	88	Y	Y
3/27	3.10	231	23.7	2.86	18.0	2.87	0.59	-0.11	1.4E6	331	153	84	N	N
3/28	3.12	224	32.6	2.93	17.9	6.04	0.24	0.15	1.6E6	292	151	99	N	Y
3/28	4.74	205	19.7	4.22	17.4	-12.4	0.01	0.55	1.3E6	298	153	101	N	N
3/28	6.36	186	13.5	3.26	17.8	-7.74	0.17	0.37	2.2E6	328	46.0	85	N	N
3/29	4.85	198	20.4	2.83	17.8	-0.65	0.06	0.56	6.8E5	330	209	77	N	N
3/29	6.45	179	19.6	2.97	17.7	-10.6	0.28	0.22	8.5E5	292	208	88	N	N
3/29	8.10	160	18.1	3.76	17.8	-9.35	0.45	-0.12	1.6E6	258	121	107	N	N
3/29	14.5	60	30.3	3.41	18.1	5.71	0.14	0.30	1.8E6	323	46.8	102	Y	Y
3/30	6.55	172	33.5	2.60	17.9	2.96	0.00	0.68	9.7E5	304	208	93	Y	N
3/30	8.15	153	32.8	2.30	18.2	17.8	0.10	0.52	1.3E6	390	253	33	Y	Y
3/30	17.8	7	33.6	2.82	18.0	10.7	0.18	0.30	1.3E6	315	93	120	Y	Y
3/31	17.9	2	31.1	3.05	18.1	1.12	0.61	-0.14	1.2E6	322	115	93	Y	Y

Table: ICON forecast studies for March, 2022.

Date UT	Time UT	Long. deg.	$V_\circ$ m/s	τ hr.	$t_\circ$ hr.	c m/s	T hr	a	I Ray.	h km	ESF obs.	ESF pred.
8/16	2.9	-118.4	12.6	2.55	19.0	-3.9	-1.55	0.84	200	290	N	N
8/17	1.3	-107.6	7.34	1.05	18.4	2.6	-1.54	1.25	200	275	N	N
8/17	3.0	-126.4	16.2	2.43	19.0	4.1	-1.37	0.94	400	290	N	N
8/17	4.6	-145.3	10.1	2.91	19.0	1.0	-1.01	1.00	270	300	N	N
8/18	4.7	-150.1	12.0	2.26	18.9	5.0	-1.27	0.93	320	310	N	N
8/18	6.3	-172.3	26.2	3.16	18.8	12.1	-1.56	0.99	210	350	Y	Y
8/19	6.4	-177.2	22.1	4.92	18.4	-10.1	-0.67	0.97	250	265	N	N
8/19	8.0	163.7	24.5	4.27	18.4	-13.7	-1.03	0.99	300	330	N	N
8/19	11.2	116.1	19.3	4.51	19.0	5.2	-0.80	1.03	600	260	Y	Y
8/20	6.4	174.9	16.4	4.65	18.3	-4.0	-	-	120	220	N	N
8/20	17.7	16.0	15.8	3.48	18.8	-1.3	-	-	130	220	Y	N
8/21	17.8	8.0	18.1	3.46	18.7	1.5	0.18	0.73	230	220	N	N
8/21	19.4	-17.4	30.0	6.03	18.2	-11.8	-0.35	0.81	430	255	N	N

Table: ICON forecast studies for August, 2022.

simulation results

Date UT	Time UT	Long. deg.	$V_\circ$ m/s	τ hr.	$t_\circ$ hr.	c m/s	T hr	a	I Ray.	h km	ESF obs.	ESF pred.
10/3	1.0	-101.1	12.6	2.62	18.3	-4.7	-0.87	0.92	-	-	N	N
10/3	2.7	-116.4	4.8	0.86	18.6	-13.3	-0.90	0.97	600	320	N	N
10/4	1.1	-104.7	24.7	2.35	18.4	22.8	-0.43	0.99	1100	320	Y	Y
10/4	4.3	-142.4	14.1	2.42	18.7	8.9	-1.10	0.92	610	350	Y	Y
10/5	2.8	-130.5	20.1	2.90	18.0	-2.2	-1.21	1.01	1000	250	N	N
10/5	4.4	-149.5	13.5	2.39	18.4	4.2	-1.22	0.59	450	325	N	N
10/5	6.0	-168.5	10.5	2.31	19.0	0.8	-1.51	0.91	420	350	N	N
10/6	4.5	-156.6	12.0	2.39	18.3	3.2	-1.36	0.38	800	300	N	N
10/6	6.1	-165.6	11.4	4.07	18.2	-2.1	-1.47	0.87	850	320	N	N
10/6	7.7	165.3	30.2	4.49	18.0	-9.1	-1.43	1.14	400	340	Y	N
10/6	12.6	95.5	11.6	1.71	18.5	16.4	-0.89	1.05	600	340	Y	Y
10/7	7.8	158.1	13.1	2.43	18.4	15.3	-1.49	1.20	850	300	Y	Y
10/7	11.0	110.6	4.8	1.12	18.4	17.3	-0.43	1.03	580	340	Y	Y
10/7	17.5	18.7	17.5	2.78	18.4	5.7	0.45	1.04	550	340	Y	Y
10/8	7.8	154.1	10.0	2.30	18.3	5.1	-1.29	0.99	850	240	N	N
10/8	9.5	128.8	23.0	2.23	18.3	24.5	-1.04	1.21	780	315	Y	Y

Table: ICON forecast studies for October, 2022.

summary

- Instability physics understood sufficiently well to reproduce irregularity behavior in simulation given suitable initialization and forcing.
- Problem then is to forecast initial plasma distribution around sunset, thermospheric winds, background electric fields after sunset.
- Can use ICON (FUV, MIGHTI, IVM) data to make forecasts one orbit in advance.
- Longer-range forecasts will require accurate PRE prediction.
- Jicamarca now acquiring ISR data almost continuously in medium-power mode.
- Cornell ionospheric model now available in ML form.
- Consider string of small satellites measuring equatorial zonal ionospheric electric fields continuously.

Bibliography

Booker, H. G. and H. W. Wells (1938). Scattering of radio waves by the F region. *Terres. Magn.*, *43*, 249

Drake, J. F., J. D. Huba, and S. T. Zalesak (1987). Finite temperature gradient stabilization of the gradient drift instability in barium clouds. *J. Geophys. Res.*, *90*, 5227–5324

Farley, D. T. et al. (1970). Equatorial spread F: Implications of VHF radar observations. *J. Geophys. Res.*, *75*, 7199

Haerendel, G. (1973). Theory of equatorial spread F. Max-Planck Institute for Physics and Astrophysics, Garching, West Germany, preprint.

Hysell, D. L., Fang, T. W., & Fuller-Rowell, T. J. (2022). Modeling equatorial F-region ionospheric instability using a regional ionospheric irregularity model and WAM-IPE. Journal of Geophysical Research: Space Physics, 127, e2022JA030513. https://doi.org/10.1029/2022JA030513

Hysell, D. L., Kirchman, A., Harding, B. J., Heelis, R. A., & England, S. L. (2023). Forecasting equatorial ionospheric convective instability with ICON satellite measurements. Space Weather, 21, e2023SW003427. https://doi.org/10.1029/2023SW003427

Hysell, D. L., Kirchman, A., Harding, B. J., Heelis, R. A., England, S. L., Frey, H. U., & Mende, S. B. (2024). Using ICON satellite data to forecast equatorial ionospheric instability throughout 2022. Space Weather, 22, e2023SW003817. https://doi.org/10.1029/2023SW003817

Kirchman, A., D. L. Hysell, & T. W. Fang (2025). Regional simulations of equatorial spread F driven with, and an analysis of, WAM-IPE electric fields. Frontiers in Physics. 10.3389/fphy.2024.1488935

Trefethen et al. (1993). Hydrodynamic stability without eigenvalues. *Science*, *261*, 578–584

Woodman, R. F., and C. La Hoz (1976). Radar observations of F region equatorial irregularities. *J. Geophys. Res.*, *81*, 5447–5466

2017 WINDY ALTAIR scans at/ prior to first sign of ESF

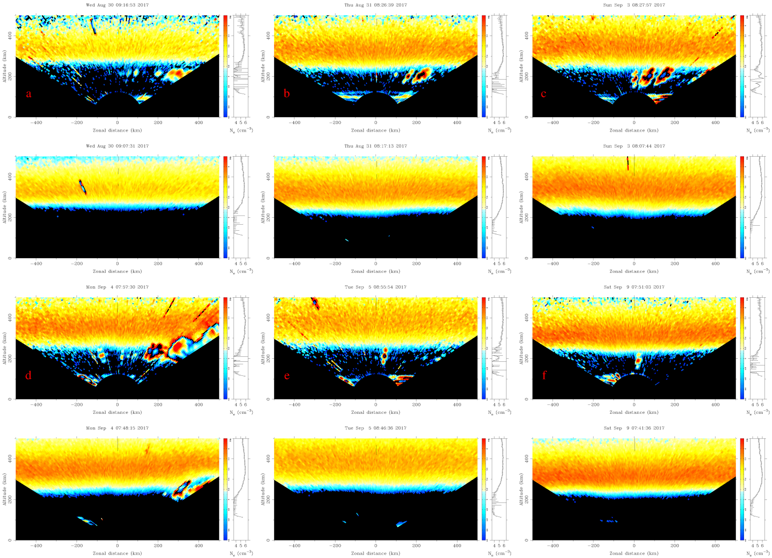

JRO medium-power mode

Max. observed plume alt. by 2100 LT (km)

Max. simul. plume alt. by 2030 LT (km)

	300	350	400	450	500	550	600	650	700
300	19	5							
350		3	2						
400			5						
450	1		2						
500			2	3	1				2
550			1	1	1				2
600				1	2			1	5
650					1		1		1
700					1				15

Table: Truth table for observed and simulated peak irregularity altitudes. Results less than 300 km and greater than 700 km are clustered together.